Sedimentary Geology 466 (2024) 106636

Contents lists available at ScienceDirect

Sedimentary Geology

journal homepage: www.elsevier.com/locate/sedgeo

Downslope evolution of supercritical bedforms in a confined deep-sea fan lobe, Amantea Fan, Paola Basin (Southeastern Tyrrhenian Sea)

E. Scacchia [a,*], R. Tinterri [b], F. Gamberi [c]

[a] Department of Earth Sciences, University of Rome Sapienza, Italy
[b] Department of Chemistry, Life Sciences and Environmental Sustainability, Earth Sciences Unit, University of Parma, Italy
[c] Istituto di Scienze Marine (ISMAR), National Research Council (CNR), Italy

ARTICLE INFO

Article history:
Received 9 January 2024
Received in revised form 27 March 2024
Accepted 28 March 2024
Available online 4 April 2024

Editor: Dr. Catherine Chagué

Keywords:
Submarine fan
Turbidity current
Facies analysis
Supercritical flow
Bedform
Hydraulic jump

ABSTRACT

The sedimentology of upper flow regime bedforms represents an important research topic at the present. Deposits interpreted as those of supercritical flows are widely recognized in modern fan systems, but their recovery is challenging. Most of the sedimentological information has come from channel thalwegs but supercritical bedforms are also frequently downslope from the channel mouths. Such an environment has been identified in the Paola basin, where erosive and depositional cyclic steps have been imaged and identified in a sandy submarine lobe of the Amantea Fan. High-resolution sub-bottom profiles provide insight into the bedform internal architecture and their relationships with a frontally-confining ridge. For the first time, supercritical bedforms in a submarine lobe have been interpreted in two distinct positions: in the scour of an erosional cyclic step and in the stoss side of a depositional cyclic step. Coarse to medium-grained massive sand with flame structures, indicating rapid sediment fall-out and frequently associated with the occurrence of hydraulic jumps, has been identified in the scour and at the toe of the ridge. The latter represents an example of topographically induced hydraulic jumps driven by a frontal confinement. Top-cut-out medium to fine sands with tractive structures have been interpreted as the deposits related to the stoss side of a cyclic step or small-scale antidune superimposed on the cyclic step surface. The presented data broaden the understanding of the range of processes that are driven by the interaction between turbidity currents and seafloor topography and the dip of the slope. The recognition that topography influences the density structure and the degree of criticality of the flow and, consequently, the morphodynamics and facies of the relative deposits may help to explain sediment distribution and improve depositional models of fan lobes in confined settings.

1. Introduction

Deep-sea fans are largely composed of packages of turbidites and contribute to the growth of sedimentary successions along continental margins (Mutti and Normark, 1987). In submarine fans, sandy depositional lobes commonly accumulate at the terminus of submarine sediment-feeder conduits, where flows lose their confinement and, eventually, a break in slope occurs. They spread unimpeded in the basin plain, creating the classical radial-shaped lobe, if the flow size is minor compared to the basin area (Normark, 1970, 1978; Shanmugam and Moiola, 1988). In contrast, where the seafloor is characterized by morphologic unevenness and the size of the flow is enough to interact with them, the spreading of sediment gravity flows can be hindered influencing flow behavior and the distribution of facies and lithology in fan lobes. The highly varied related deposits have been investigated both in modern (Deptuck et al., 2008; Gamberi et al., 2014) and ancient confined basins (Kneller et al., 1991; Kneller and McCaffrey, 1999; Amy et al., 2004; Remacha et al., 2005; Tinterri and Tagliaferri, 2015; Tinterri et al., 2017, 2022; Tinterri and Civa, 2021) and by relevant experimental analogs (Kneller, 1995; Amy et al., 2004; Nasr-Azadani et al., 2013; Nasr-Azadani and Meiburg, 2014; Patacci et al., 2015; Howlett et al., 2019; Soutter et al., 2021).

A flow is supercritical when its velocity exceeds the influence of gravity, and this relation is expressed by the Froude number (*Fr*) that, for open-channel flows, coincides with $Fr > 1$; while, for density flows, it can be non-unity or non-existent (Huang et al., 2009). Compared to open-channel flows, density flows (i.e. turbidity currents) can reach supercritical conditions even with low flow velocity since the buoyancy force reduces the influence of gravity (Komar, 1971; Sequeiros, 2012). For this reason, supercritical bedforms are widely recognized in modern and ancient marine systems. The majority of the

* Corresponding author.
E-mail addresses: elena.scacchia@uniroma1.it (E. Scacchia), roberto.tinterri@unipr.it (R. Tinterri), fabiano.gamberi@bo.ismar.cnr.it (F. Gamberi).

https://doi.org/10.1016/j.sedgeo.2024.106636
0037-0738/

supercritical bedforms (i.e. antidune and cyclic step end members) may result from rapidly-moving high-density stratified flows (Postma et al., 2009; Postma and Cartigny, 2014; Hughes Clarke, 2016; Fildani et al., 2021). In fact, the progressive increase of the basal density, leading to the consequent formation of a bipartite stratified flow, led to the downward expansion of the supercritical flow domains in the bedform stability field due to the suppression of the turbulence (Cartigny and Postma, 2017). Antidunes form through supercritical turbidity currents, while cyclic steps are related to alternating flow regimes since each step is bounded at its upstream and downstream ends by a hydraulic jump, a short zone over which the flow experiences a rapid transition from shallow and supercritical to thick and subcritical (Fildani et al., 2006; Cartigny et al., 2014; Fedele et al., 2016; Cartigny and Postma, 2017; Covault et al., 2017; Kostic, 2011, 2014; Slootman and Cartigny, 2020). Cyclic steps are generally classified as net-erosional or net-depositional, depending on whether erosion or deposition dominates across the bedforms (Cartigny et al., 2011, 2014). Net-erosional cyclic steps are manifested as scours, whereas net-depositional cyclic steps take the form of upstream-migrating sediment waves (Cartigny et al., 2011; Fildani et al., 2006; Kostic, 2011; Spinewine et al., 2009). Cyclic steps and antidunes, eventually comprising the intermediate terms (chutes-and-pools and unstable antidunes), may form a downflow succession of bedforms recording how flow conditions change in space (Lang and Winsemann, 2013; Cartigny et al., 2014; Zhong et al., 2015) while how they are stacked vertically represents how the flow conditions change over time (Kostic, 2014; Lang et al., 2017a, 2017b; Kostic et al., 2019). Recognition of supercritical deposits in outcrops is challenging but fossil, on-land examples of cyclic steps have been extensively identified and described. Thus, the sedimentology of upper flow regime bedforms has been described more frequently in outcrop (Cartigny et al., 2014; Postma et al., 2009, 2016; Gong et al., 2017; Lang et al., 2017a, 2017b; Ono and Plink-björklund, 2018; Postma and Kleverlaan, 2018; Cornard and Pickering, 2020; Ono et al., 2021) than in the deep modern marine environment. The difficulty of sampling supercritical bedform deposits on the seafloor, where they are frequently recognized in proximal fan settings (channel thalweg, channel–lobe

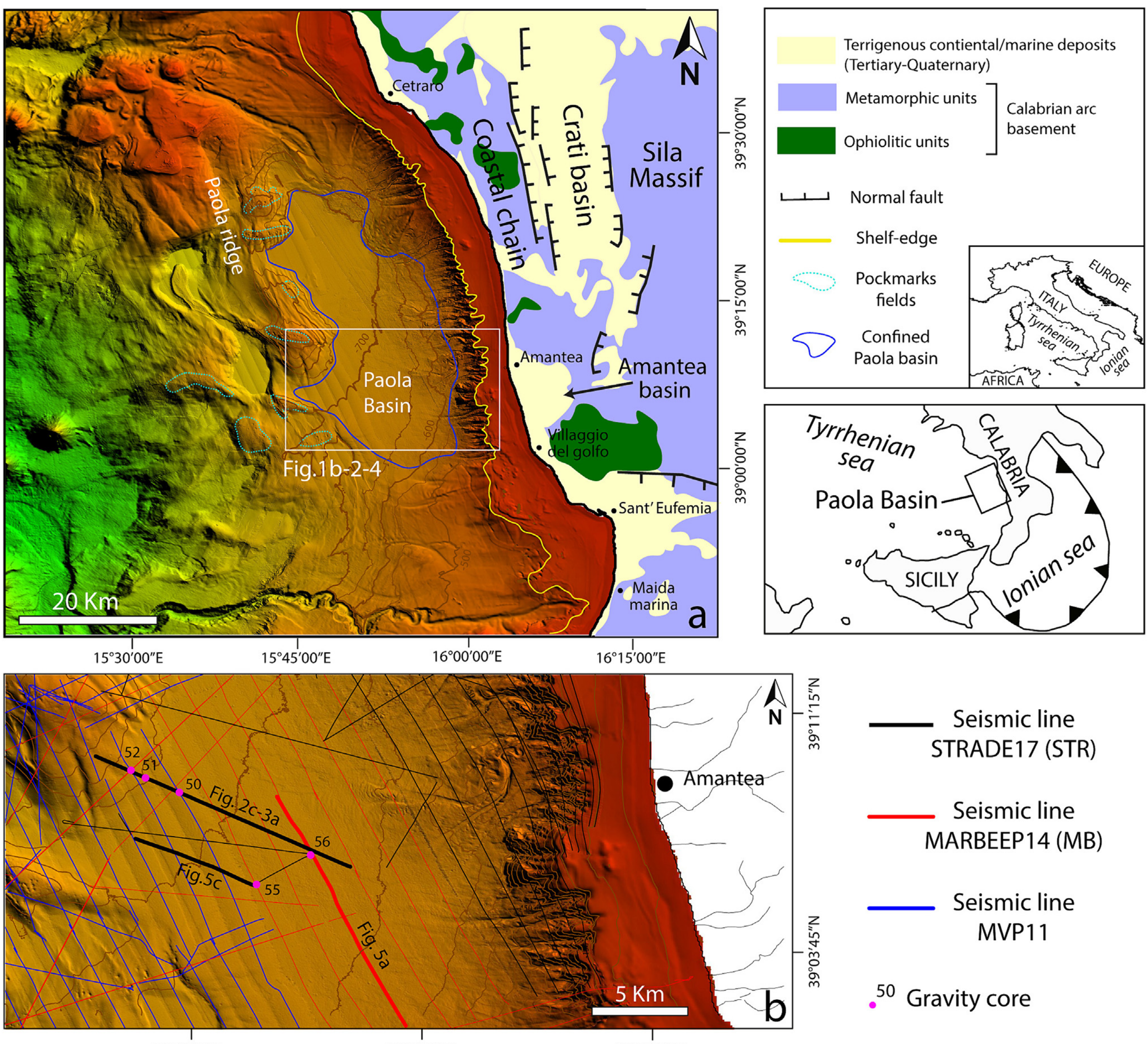

Fig. 1. (a) Shaded relief map of the Paola Basin, with contour lines spaced at 50 m (see location within the Tyrrhenian subduction system in the inset). The study area corresponds with the area in the white box. (b) Shaded relief map of the study area with the location of the CHIRP profiles and of the gravity cores. The bold black and red lines correspond to the segments of the CHIRP profiles shown in Figs. 3 and 5. The different colors of the CHIRP lines correspond to different acquisition surveys as shown in the upper left legend.

transition zone, proximal lobe) where the coarsest grain-sizes settle down, accounts for this mismatch (Hughes Clarke et al., 1990; Postma et al., 2009, 2014; Ono and Plink-björklund, 2018; Ono et al., 2021). In fact, at present, very few seafloor sediment samples are available to pinpoint the sedimentology of cyclic steps, and they are prevalently located in channel thalwegs (Fildani et al., 2006; Hage et al., 2018). However, what are interpreted as upper flow regime bedforms are also frequently identified downslope from the channel mouths, as shown by most of the above cited outcrop studies.

In the Tyrrhenian Sea, supercritical flows and relative upper flow regime bedforms form preferentially in the steep slope environment where canyon heads are generally connected with short subaerial drainage systems and narrow shelves (Casalbore et al., 2014, 2017; Bosman et al., 2017; Lo Iacono et al., 2017; Scacchia et al., 2022). In this setting, swift sand-rich high-density turbidity currents flow on high-gradient slopes and basin floors. Such an environment in the Paola intraslope Basin, located in the Calabrian margin, the southern portion of the Italian peninsula, is investigated in this paper.

In the Paola basin, erosive and depositional bedforms have been imaged and sampled in a sandy submarine lobe of the Amantea Fan (Fig. 1). High-resolution sub-bottom profiles provide insight into the internal architecture of the lobe and its relationships with a frontally-confining ridge (Paola Ridge). The main objectives of this paper are to: i) Characterize the different depositional and erosional elements that compose the lobe through seismo-stratigraphic observations and sedimentologic facies analysis and ii) interpret the downflow changes of the bedforms and the behavior of their parent flow. Our findings wish to bridge the resolution gap between outcrop studies and morphodynamic studies in modern systems and may help in evaluating the results from recent flume tank experiments. The description and manipulation of the data, results, and related interpretations presented in this paper have been revised based on the Ph.D. thesis of the corresponding author (Scacchia, 2023).

2. Geological setting

The Paola Intraslope Basin is 60 km long (about 700 km^2), and trends NNW–SSE along the eastern Calabrian margin, in the offshore between the towns of Cetraro and Sant'Eufemia (Fig. 1a). It has a narrow shelf and steep slope that connects with the basin plain at a depth of around 700 m. The Paola Basin is a confined, margin-parallel trough (Gamberi et al., 2019) bounded seaward by the Paola Ridge (Fig. 1a) interpreted by Gamberi and Rovere (2010) as the surface expression of a mobile mud belt, connected to a set of extensional faults trending NW–SE to NNW–SSE while other authors interpreted those structures as transcurrent faults (Milia et al., 2009; Corradino et al., 2020). The Paola ridge hosts cold seep structures identified as large fields of pockmarks (Gamberi and Rovere, 2010; Rovere et al., 2014, Fig. 1a).

The Coastal Chain, a mountain range located in the western part of Calabria is the source of sediment for the Paola Basin and is composed of ophiolitic and crystalline basement unconformably overlapped by Tertiary to Quaternary sedimentary deposits (Fig. 1a). The Coastal chain is carved by steep and short rivers with torrential regimes, locally known as Fiumara streams (Sabato and Tropeano, 2004). Flash floods periodically occur within these short-rivers, and, in entering the sea, can originate hyperpycnal flows and transport a large amount of debris into the sea (Casalbore et al., 2011).

The continental shelf is generally narrow (2 km) and steep (1°–2.5°) (Fig. 1a). Beyond the shelf break, located at 140–150 m depth, several small canyons often indent the shelf break and deeply incise the continental slope (Fig. 1a). They usually have straight courses and develop down to the base of the slope, at about 650–700 m of depth. The basin floor is confined to the west by the counter-slope of the Paola ridge and deepens to the north. It reaches about 12 km in width to the south and narrows to 8 km northward. The southern portion of the basin is the focus of this study (Fig. 1b).

The Paola basin infill is composed of a Plio-Quaternary sequence that reaches a maximum thickness of about 5 km and consists mostly of turbidite deposits that onlap on the Paola Ridge (Trincardi et al., 1995; Milia et al., 2009; Gamberi et al., 2019). Vertically stacked, highly reflective mounded and channelized deposits indicate the recurrence of turbidity currents associated with sediment input mainly occurring during the low-stand periods. Mass-transport deposits and hemipelagic sedimentation form drapes and intercalations, with acoustically transparent seismic facies, within the turbidite succession. The most recent of the drapes consists of late Quaternary sediment, which correlates with the transgressive and highstand deposits on the shelf (Trincardi et al., 1995).

3. Methods

Multibeam bathymetric data, high-resolution CHIRP sub-bottom profiles and gravity cores represent our dataset. A major part of the study area is covered by a digital high-resolution terrain model. The latter consists of a mosaic of multibeam data acquired during three oceanographic surveys carried out in 2011, 2014, and 2017 (MVP11, MARBEEP14 and STRADE17 respectively, Fig. 1b). The first two cruises were carried out on board the R/V Urania equipped with the multi-beam system Kongsberg EM710 (frequency 70–100 kHz). In general, given the frequency of the multibeam instruments and the depth range of the study area, the bathymetric data have a vertical resolution of <0.5 m. During the cruises, the bathymetric soundings were carried out between 300 and 1300 m of depth. The shallowest areas, from 700 m to 150 m depth, were investigated recently during the cruise STRADE17 executed with the R/V Minerva UNO vessel with the multibeam system Seabat7160 (frequency 44 kHz) with a resolution of about 0.5 m. The acquired data has been merged with the EMODnet Project bathymetric data available on the continental shelf. The multibeam bathymetric data were imported and analyzed using the Global Mapper® software for the production of contour and slope maps. High-resolution subbottom data consists of CHIRP (Compressed High Intensity Radar Pulse) profiles, collected using the CHIRP Benthos 179 III technology (frequency 2–7 kHz). Their location is shown in Fig. 1b. This system penetrates up to 100 m in the sub-seafloor sediment, with a vertical resolution in the order of 0.5 m. Observations from high-resolution profiles are combined with the sedimentologic interpretation of five gravity cores. The cores penetrated the surficial sediments down to a depth of about 5 m and have been analyzed in order to infer the detail of the depositional processes involved in bedform formation. Three gravity cores have been acquired in the basin floor (56–55-50) and two on the Paola ridge (51–52) (Fig. 1b). Cores were split lengthwise, photographed with a digital camera, and detailed with visual sedimentological descriptions. The sedimentological characterization focused on bed thickness, grain size (according to the Udden–Wentworth grain-size scale, Wentworth, 1922), sedimentary structures, bioturbation, description of volcanic products (femic tephra, pumice), and accessory elements (i.e. presence of bioclast, foraminifera, ichnofossil, oxidized layer).

4. Results

4.1. Morphological features in the study area

On the continental margin of the Paola Basin, the bathymetric data show a complex physiography resulting from the presence of several distinct morphologic features (Fig. 2). In the northern part of the study area, numerous landslides, shown by widespread erosional features, involve the upper slope sediment, and their deposits extend downslope to about 700 m of depth (Fig. 2). In front of the Amantea town, distinct shelf-break indentations are the heads of two canyons named the Licetto and the Oliva Canyons, from the homonymous rivers locally called "*fiumare*" flowing to the coast (Fig. 2). The connection between "*fiumare*" (i.e. rivers whose catchments developed mainly in high mountain areas and characterized by episodic catastrophic flash floods)

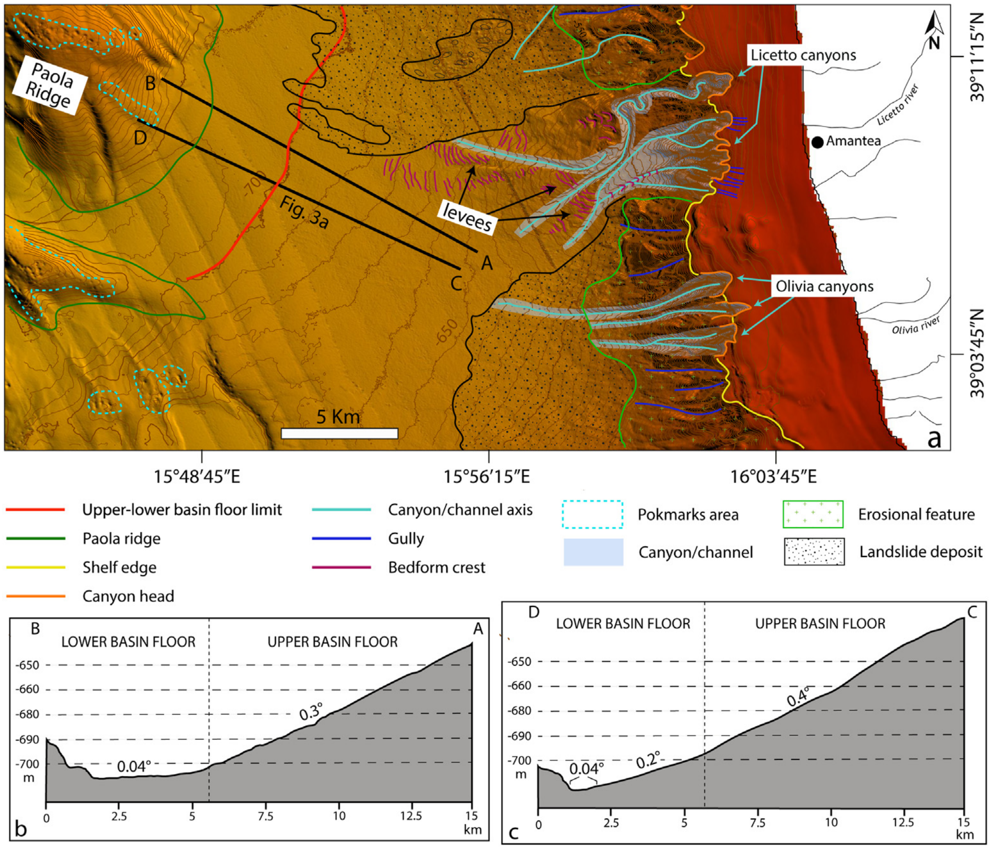

Fig. 2. (a) Map of the morphological elements in the study area. Contour line spacing is 10 m. (b–c) Seafloor profiles show the physiography of the basin floor, where the upper basin floor is broadly 0.3–0.4° steep. While the lower basin floor is almost flat (0.04°) to the north (profile A–B in b) and halved (0.2°) to the south (profile C–D in c).

and canyon systems is widely recognized in the Calabrian margin (Casalbore et al., 2011; Gamberi and Marani, 2006, 2008). In fact, landward from the head of the Licetto Canyon indentations, gullies are present in the shelf, which, due to the indentation, narrows to 2 km. Similar gullies have been identified in other systems of the Tyrrhenian Sea and were interpreted to be related to flash-flood hyperpycnal flows, favored by steep drainage basins and torrential regimes (Clementucci et al., 2022). In the area of the Licetto Canyon, the upper slope dips at about 8–10°, while the lower slope dips at about 1.5°. In the lower slope, all the canyons evolve into straight channels bounded by levee deposits with depositional bedforms (Fig. 2). To the south of the Amantea town, the shelf break is carved by three canyon heads of the Oliva canyons. Only the northern of them is connected through a channel to the lower slope (Fig. 2). Here the upper slope is less steep compared to the northern areas, reaching about 5–7° while the lower slope dips at 1.5°. The basin floor, between the base of the slope and the base of the Paola ridge, can be subdivided into two sectors, an upper and lower basin floor, according to the slope value. The upper basin floor occurs from 650 to 700 m of depth, and dips at about 0.3–0.4°, while in the lower basin floor, downslope from 700 m of depth, the slope is reduced. To the north, the lower basin floor is almost flat, dipping on average at 0.04° (Fig. 2b), while to the south is steeper (0.2°) but halved compared to the slope value in the upper basin floor (Fig. 2c). A saddle in the Paola ridge forms a corridor that connects the Paola basin to a deeper intraslope basin.

4.2. Seismic stratigraphy

4.2.1. Acoustic facies

Taking into account the presence or absence of reflections, their relative amplitude and their geometry (parallel, irregular, etc.), five different acoustic facies have been distinguished. In our seismic facies classification, the first word describes the reflection geometry (parallel or irregular) or their absence (transparent facies); the second word describes the strength of the acoustic reflection (high or low amplitude):

Transparent Low-reflectivity (TL) Intervals lacking coherent reflections with faint reflectivity.
Parallel Low-reflectivity (PL) Parallel to subparallel low-amplitude reflections.
Parallel High-reflectivity (PH) Parallel to subparallel high-amplitude reflections.
Convex High-reflectivity (CH) Large and small-scale convex-shaped high amplitude reflections.
Structureless High-reflectivity (SH) Intervals lacking continuous reflections with high reflectivity, commonly reducing the penetration of acoustic energy.

4.2.2. Seismic profile interpretation

The upper 20 m of stratigraphy consists of six units: Drape 1, MTD 1, Amantea Fan, MTD 2, Drape 2 and Drape 3, each characterized by a specific acoustic response (Fig. 3). The Amantea lobe corresponds with a strongly reflective unit, sandwiched between faintly reflective (TL) units (Fig. 3). Its seismic facies most likely indicates coarse-grained stratified deposits, corresponding to the deposits of turbidity currents. Conversely, the acoustically transparent units are generally associated with homogeneous fine-grained deposits and, when their distribution is uniform throughout the study area, have been interpreted as hemipelagic drape deposits (Drapes 1–2–3). When they form local bodies, not continuous over the whole area, they have been interpreted as mass-transport deposits (MTDs 1–2).

The Amantea Fan lobe extends from the upper basin floor to the lower basin floor, where it reaches the maximum thickness of 7.5 m at the base of the Paola ridge, while it gradually thins and finally pinches

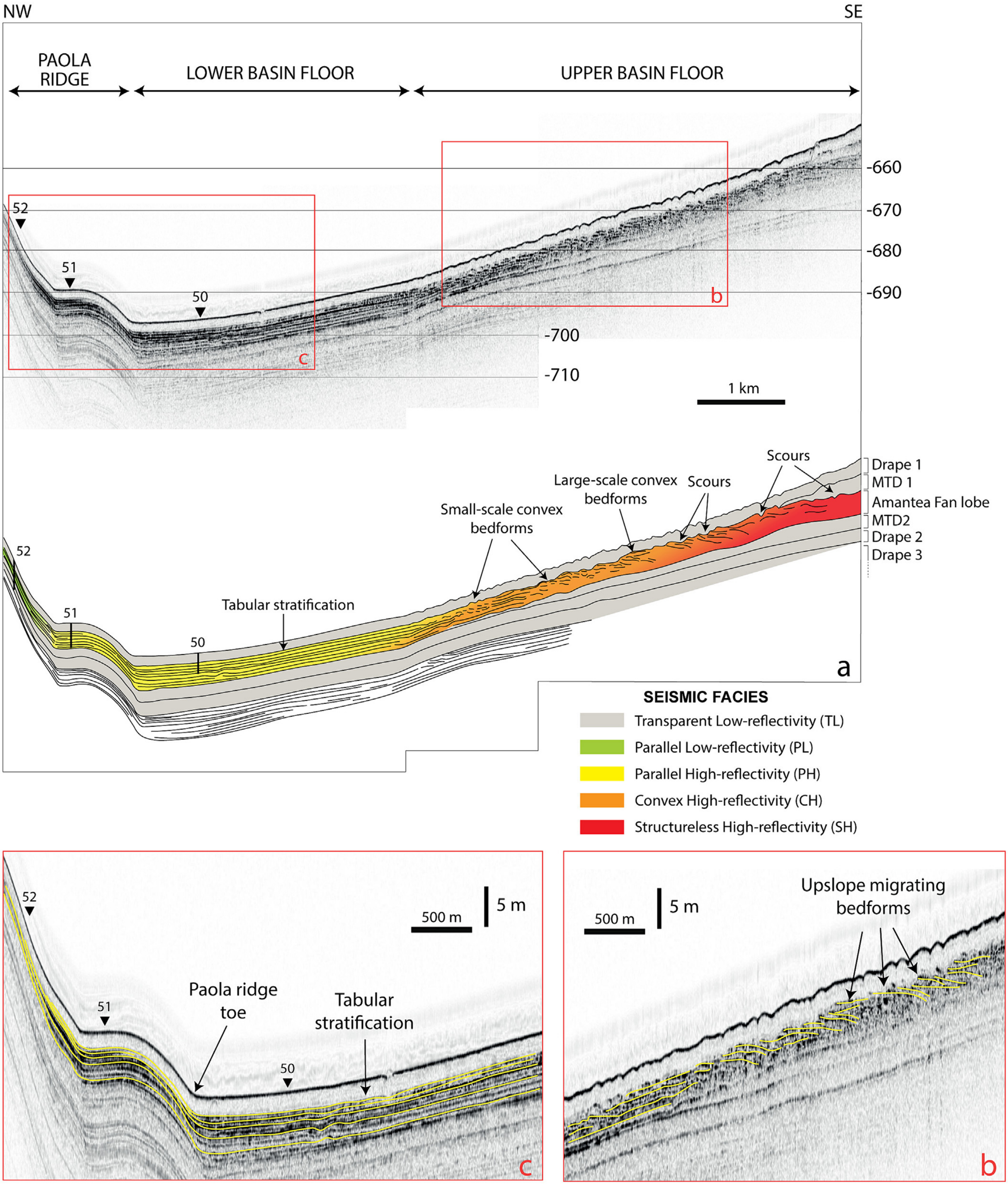

Fig. 3. (a) CHIRP profile (profile track is reported in Fig. 1a and cross-section in Fig. 2c) crossing the upper and lower basin floor and the Paola Ridge in a WNW–ESE direction. Below the interpreted line drawing of the principal reflectors and the units comprised between them and the seismic facies are marked by colors. (b) Detail of the upslope migrating bedforms in the upper basin floor. (c) Detail of the tabular beds in the lower basin floor and on the surface of the ridge, the exact location of gravity cores (50–51–52) is reported.

out westward onto the Paola ridge (Fig. 3). Its extent, as reconstructed through the seismic profiles, amounts to about 240 km^2; it pinches out to the south and spreads to the north (Fig. 4). The eastern limit of the fan lobe is uncertain since the overlying mass-transport deposits on the upper basin floor reduce the penetration and the resolution of the seismic profiles (Fig. 4).

In the upper basin floor, the fan pinches-out toward the SE and thickens toward the NW (Fig. 5a). In the same position of Fig. 5a, the

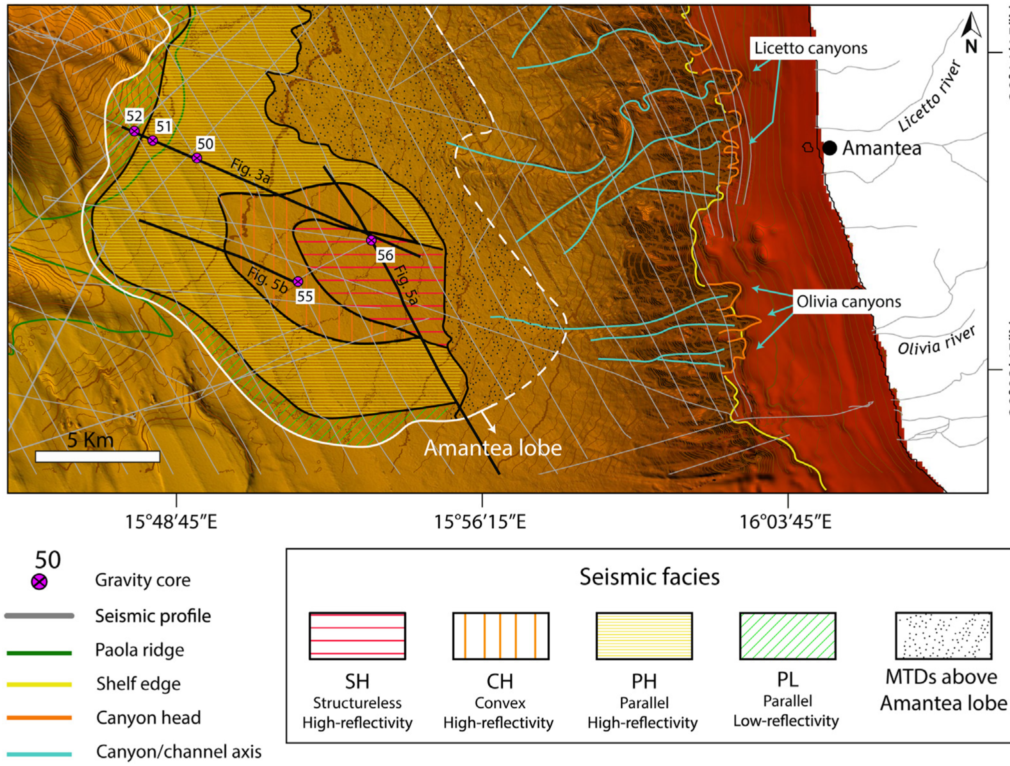

Fig. 4. Amantea lobe and its seismic facies distribution through the study area. Note the preferential orientation of the SH and CH seismic facies toward NW. Available seismic profiles and gravity cores are reported as well as the principal morphological elements.

fan forms a 5 m-thick body with mounded morphology and internally presents high-amplitude seismic facies (SH). Only some small-scale depressions truncate the reflectors of the upper portion of the Amantea fan unit. They are interpreted as scours (Fig. 5a–b) which are 150 m long and <1 m deep.

Downslope, the lobe has a wavy surface (Figs. 3a, 5c) and CH facies and is arranged in distinct depositional bodies interpreted as a train of depositional bedforms. The internal reflections dip toward the SE, highlighting the upslope direction of migration of the bedforms (Figs. 3a–b, 5c–d). In section view, bedforms have a steep lee side and gentle stoss side resulting in asymmetric bedforms with about 100–200 m wavelength and 1 m of amplitude.

The distribution of both the SH and CH facies in the Amantea fan lobe clearly outlines a depositional area elongated in a NW–SE direction (Fig. 4). Moreover, bedform cross-sections, that are parallel to the flow direction, are directed toward the NW (Fig. 3). This shows a direct connection with flows exiting the Oliva canyon and channel system, whose distal part is close to the proximal part of the mapped Amantea fan lobe (Figs. 2 and 5). The SE–NW direction is thus assumed as the lobe axis region. However, a contribution from the Licetto Canyon is also possible since the mouths of the southern channels of the system are located upslope from the Amantea fan lobe.

4.3. Sedimentological analysis

4.3.1. Reference facies scheme

The sedimentological analysis of 5 gravity cores in the Amantea lobe has been interpreted within two reference facies schemes: the one elaborated by Postma and Cartigny (2014) reporting the facies association produced by a depositional cyclic step and the facies scheme from Tinterri et al. (2023) that links the sedimentological facies to flow criticality (Fig. 6). The facies scheme by Postma and Cartigny (2014) distinguishes high- and low-density flow deposits and their sedimentary structures as a function of the Froude number and fallout rate. The scheme from Tinterri et al. (2023), based on the facies scheme of Mutti (1992) and Mutti et al. (2003), represents the ideal facies tract recorded by a bed deposited by a single sediment gravity flow undergoing transformations (i.e. flow regime) during its basinward motion. There is good correspondence between the two facies schemes, but the latter includes a further subdivision based on grain size and for this reason, it will be the reference facies scheme in our paper. In particular, the principal facies are coarse (F5f) or medium (F8f) massive sand with flame structures; coarse (F5m) or medium (F8m) massive sand, coarse (F7) or medium (F8cl) sand with spaced lamination (>0.5 cm); medium sand with plane lamination (<0.5 cm) (F8l) and fine sand with plane lamination and ripple (F9) (Fig. 6).

4.3.2. Gravity-core sedimentology

Two cores (56 and 55) sampled the upper basin floor, one core (50) sampled the lower basin floor, and two cores (51 and 52) sampled the Paola ridge (Fig. 1b). Cores 55 and 56 form a 3.1 km long SW–NE oriented transect perpendicular to the flow direction (Fig. 7) in the upper basin floor, and cores 56, 50, 51 and 52 form a 9.6 km long NW–SE-trending downflow transect that crosses the basin floor and onto the Paola Ridge along the CHIRP line of Fig. 3 (Fig. 8). The upper part of all the cores consists of Drape 1 muddy sediment (Figs. 7–8). Within Drape 1, the 79 CE tephra layer (tephra layer 1) of the Plinian eruption of Mount Vesuvius (Trincardi et al., 1995) forms a 2 cm thick layer composed of femic black fragments with a medium grain-size, 30 cm b.s.f. (Figs. 7–8). Below Drape 1, the onset of sandy layers marks the turbidites of the upper part of the Amantea fan lobe. Another tephra bed (tephra layer 2) interlayered between turbidite beds 2 and 3 of the fan lobe, consisting of femic tephra and pumice fragments, represents a deeper key layer that supports the core-by-core correlation. Since the core location is along sub-bottom profiles, their facies associations can be tied to specific morphologic elements of the fan.

4.3.2.1. Gravity core 56 (scour). Core 56 sampled the trough of a scour in the proximal lobe area (Fig. 5b) where the Amantea fan lobe presents SH seismic facies (Fig. 4). The Amantea Fan lobe deposits, below Drape

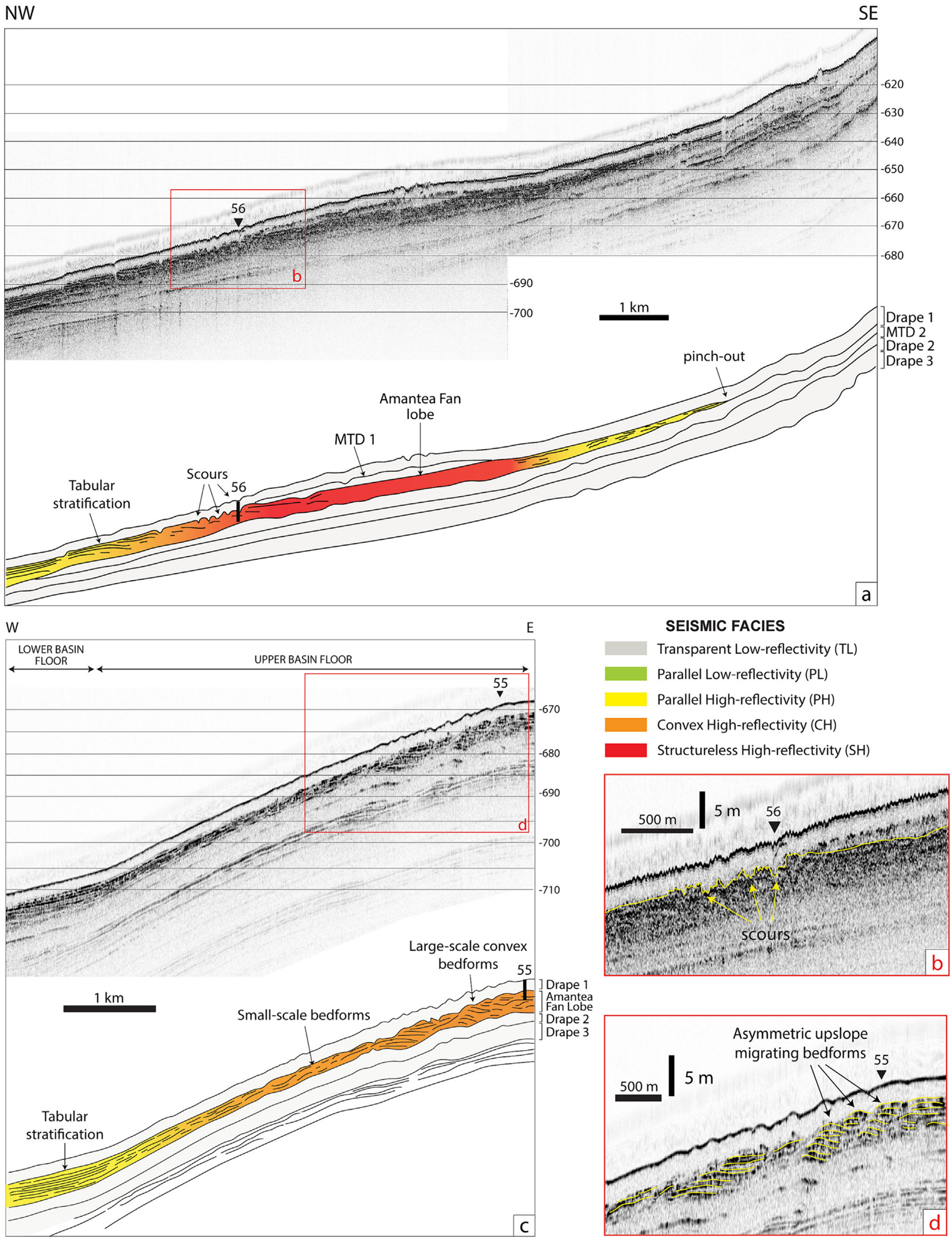

Fig. 5. CHIRP profile (profile track is reported in Fig. 1a), and below the interpreted line drawing of the principal reflectors and the units comprised between them and the seismic facies are marked by colors. (a) CHIRP profile crossing the upper basin floor. Note the pinching of the lobe toward SE and the presence of scours toward NW. The red rectangle (b) contains the details of the scours where a sample (56) has been acquired. (c) CHIRP profile crossing the upper and lower basin floor. The red rectangle (d) highlights the detail of the upslope migrating bedforms in the upper basin floor characterized by CH seismic facies, a gravity core (55) sampled the stoss side of one of those bedforms.

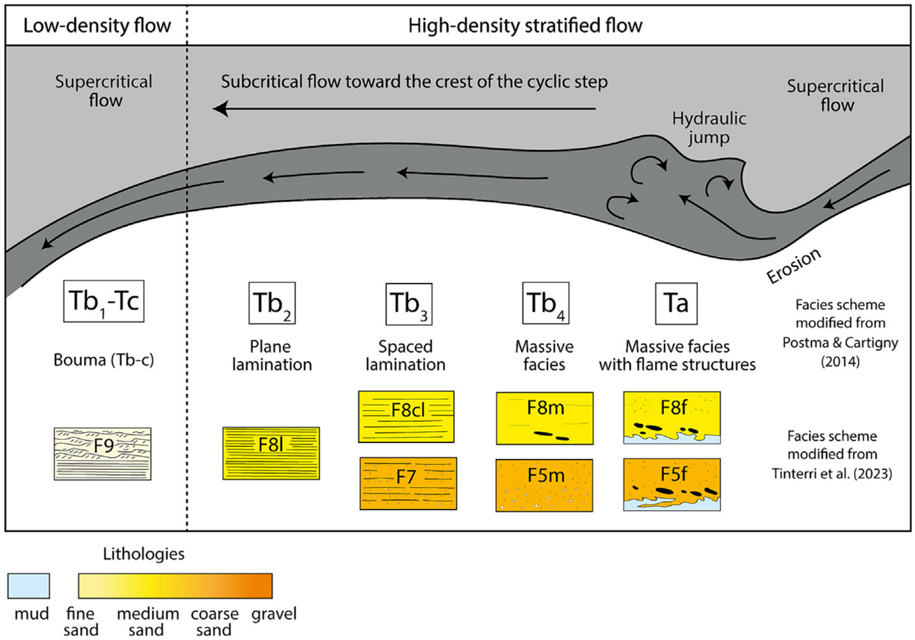

Fig. 6. The facies scheme by Postma and Cartigny (2014) and Tinterri et al. (2023). The latter allows more detailed classification with emphasis on the grain sizes of the different facies. (Modified from Postma and Cartigny (2014) and Tinterri et al. (2023).)

1, consist of very thin (2 cm) to thick (45 cm) turbidite beds composed of very coarse to medium-grained sand (Fig. 7a). Two thin-bedded top-cut-out (sensu Walker, 1965) coarse-grained turbidites with a slightly erosive base (turbidites 1 and 2, Fig. 7b) are below the tephra layer 2. Turbidite 2 presents inversely graded (highlighted with red arrows in Fig. 7b) parallel-spaced laminations of very coarse-grained sands (F7) interpreted as deposited by traction carpets (sensu Lowe, 1982; Hiscott, 1994; Sohn, 1997). Turbidite 3, above the tephra layer 2, has an erosional base that scours the substrate, reworking the underlying tephra layer and shows flame structures (Fig. 7b). It has a massive, basal interval of medium-grained sand (F8f) and a laminated top (F8l) (Fig. 7b). Turbidite 4 has an erosional base and is composed of very coarse-grained massive sand with mudclasts (F5f) occurring at the base and near the top (Fig. 7b). An abrupt grain-size increase, associated with aligned mudstone clasts, marks an amalgamation surface that is the base of turbidite 5. The latter is composed of massive very coarse to coarse-grained sandstone. Turbidites 1, 2, 3 and 5 are characterized by sharp tops with evident grain-size breaks (i.e., the upper fine-grained laminated portions are absent).

4.3.2.2. Gravity core 55 (bedform stoss side). Core 55 sampled the stoss side of one of the upslope-migrating bedforms in the proximal lobe area with CH seismic facies (Figs. 4 and 5d). Here, turbidites 3, 4 and 5 are medium/fine-grained with thickness ranging from thin- (8 cm) to thick-bedded (37 cm) (Fig. 7a). The base of the turbidites is sharp (turbidite 3 and 4) or slightly erosive (turbidite 5) and some chondrite trace fossils occur at the base of turbidite 4. Turbidites 3, 4 and 5 have a massive fine-grained basal sand (F8m) capped by parallel laminations and ripples (F9, Fig. 7c) and turbidite 5 presents mudclasts at the top. The silt fraction is absent in all the turbidites and consequently, the beds pass upward into a clay division through a sharp contact (top-cut out-bed, Fig. 7c).

4.3.2.3. Core 50 (frontally-confined tabular beds). The core sampled the distal lobe area, in the lower basin floor, where tabular beds with PH seismic facies occur (Figs. 3c and 4). Turbidites 2, 3 and 5 are composed of medium-grained sand and have an almost constant thickness of about 15 cm (medium-thick beds) (Fig. 8a). These beds are normally graded with massive basal facies made up of medium-grained sand with small flame structures in turbidites 2 and 5 (F8f), and sporadically pumice laminae are found (turbidite 3); these basal divisions pass upward into fine-grained sandstones and siltstones (F9) (Fig. 8b). The base of beds 2, 3 and 5 is erosional or slightly erosional (Fig. 8b).

4.3.2.4. Cores 51 and 52 (turbidites approaching the pinch out: beds on Paola Ridge). Cores 51 and 52 sampled the proximal part of the Paola Ridge (Fig. 3c). Core 51 sampled the PH facies of the Amantea fan (Fig. 4), consisting of thin-bedded fine-grained turbidites (turbidites 1, 2, 3, 4 and 5, Fig. 8a). The latter are mainly plane-parallel laminated and normally graded beds with a sharp base (F9, Fig. 8c). Core 52 sampled the PL facies of the Amantea fan lobe (Fig. 4). The core correlation (Fig. 8a) and the picking of the reflector in the seismic profile reveal that the tephra layer 2 is the only bed present in core 52 that is also present in the other cores.

The sedimentological analysis of the cores combined with the seismic facies interpretation allowed the calibration of the lithology with the seismic facies (Table 1).

5. Discussion: from the data to the flow dynamics

Recent experimental and field studies have indicated that sub- and super-critical turbidity currents can be distinguished on the basis of the nature of their sedimentary products and specific facies associations (Postma and Cartigny, 2014; Lang et al., 2017a, 2017b; Hage et al., 2018; Cornard and Pickering, 2019; Postma et al., 2021; Tinterri et al., 2023). In the Amantea Fan lobe, some of the turbidites have characteristics that match the facies association recognized as typical of supercritical flows (Fig. 6). Sedimentary structures occurring in the scour (turbidite 2 in core 56, Fig. 7b) consist of thin-bedded top-cut-out beds with very coarse-grained traction carpets. The traction carpets can be associated with tractive rapid flows, related to high-density turbidity currents (Lowe, 1982; Hiscott, 1994; Sohn, 1997; Postma et al., 2009; Lang et al., 2017a; Tinterri et al., 2023). According to Postma et al. (2009), traction carpets can form under both super and subcritical flows, and they can be discriminated since in the first case traction carpets are deposited as large back sets that cannot be detected from cores. Turbidite beds 3, 4 and 5, in the trough of the scour located parallel to the principal flow direction, are characterized by massive, coarse-graded sediments with flame structures and other deformed and reworked sediment (i.e. mudclasts) (Fig. 7b). The described facies and related sedimentary structures, indicative of rapid fall-out values, have been frequently interpreted as the sedimentary signature of hydraulic jumps (Postma et al., 2009, 2014; Postma and Cartigny, 2014; Tinterri et al., 2016, 2023; Lang et al., 2017a; Hage et al., 2018; Ono et al., 2021). Scour

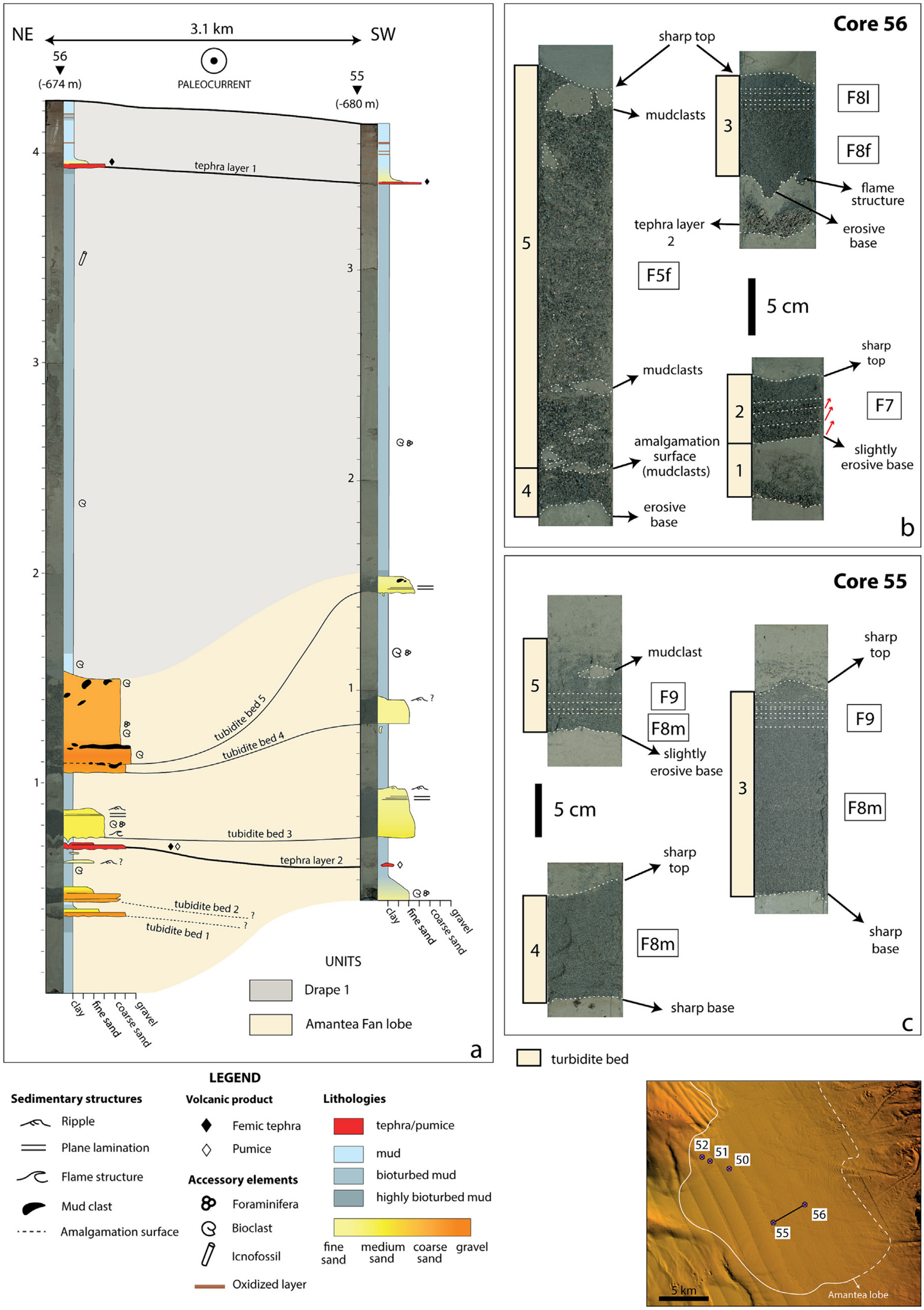

Fig. 7. Correlation of cores 56–55 (locations in Fig. 1b). Core 56 shows predominantly coarse-grained turbidite beds while core 55 presents medium to fine-grained turbidite beds. Detail of the turbidite beds of cores 56 (b) and 55 (c) and relative sedimentary structures. Turbidite bed numbers are indicated in the yellow boxes to the left of the core photographs.

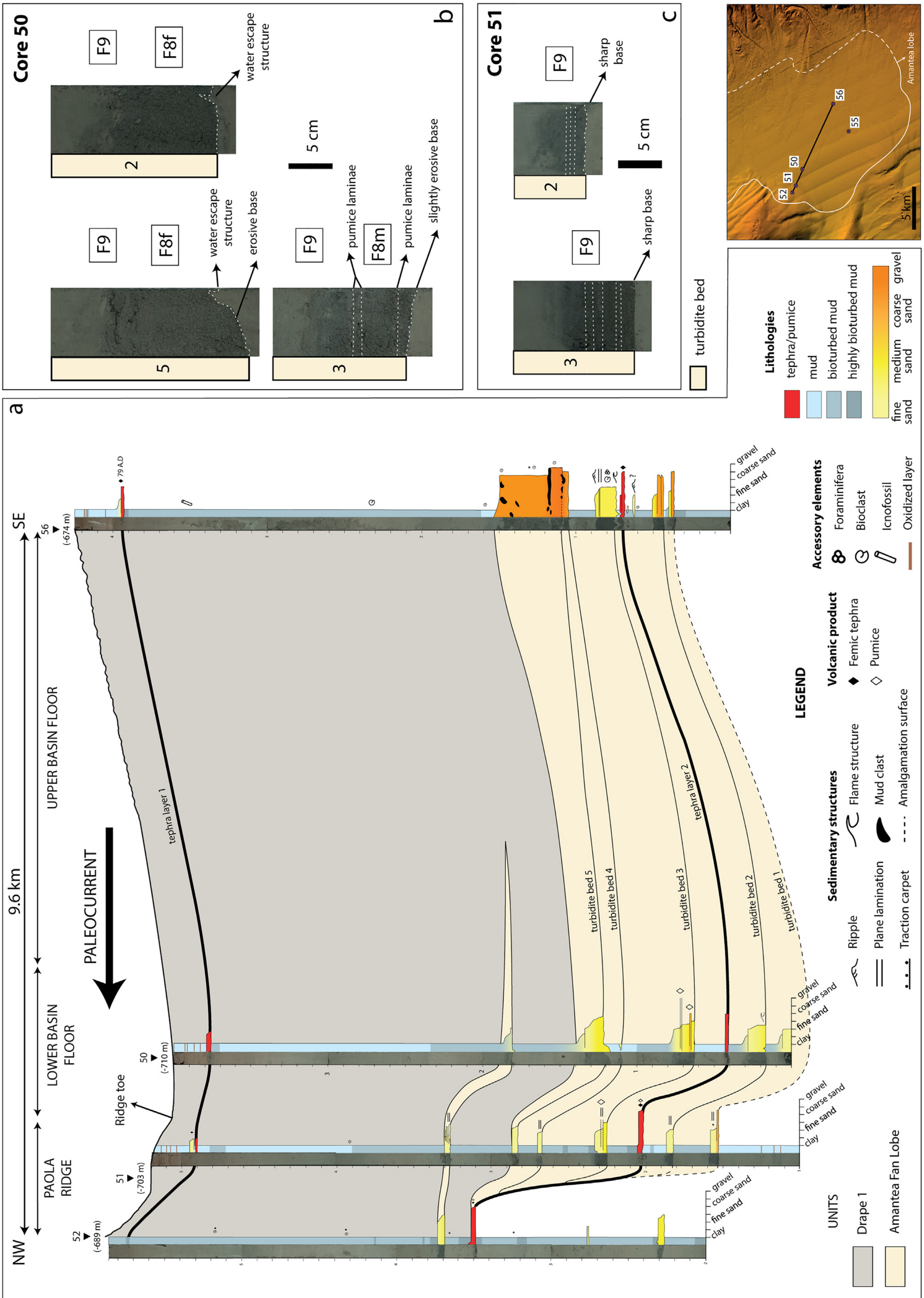
a
NW
SE
9.6 km
PAOLA RIDGE
LOWER BASIN FLOOR
UPPER BASIN FLOOR
Ridge toe
PALEOCURRENT
52 (-689 m)
51 (-703 m)
50 (-710 m)
56 (-674 m)
79 A.D
tephra layer 1
tephra layer 2
turbidite bed 5
turbidite bed 4
turbidite bed 3
turbidite bed 2
turbidite bed 1
clay
fine sand
coarse sand
gravel
UNITS
Drape 1
Amantea Fan Lobe
LEGEND
Sedimentary structures
Ripple
Plane lamination
Traction carpet
Flame structure
Mud clast
Amalgamation surface
Volcanic product
Femic tephra
Pumice
Accessory elements
Foraminifera
Bioclast
Icnofossil
Oxidized layer
Lithologies
tephra/pumice
mud
bioturbated mud
highly bioturbated mud
fine sand
medium sand
coarse sand
gravel
b
Core 50
F9
F8f
water escape structure
erosive base
F8m
pumice laminae
slightly erosive base
5 cm
c
Core 51
sharp base
turbidite bed
Amantea lobe
5 km

Table 1
Summary of the depositional and erosional elements recognized according to their seismic facies and relative lithological interpretation derived from the sedimentological description of gravity cores sampling the elements.

Depositional/erosional element	Unit	Setting	Seismic facies	Seismic facies description	Sample	Sample lithological description
Hemipelagic drape	Drape 1	Expanded all throughout the study area	TL	Transparent, faintly reflective	56–55–50–51–52	Relatively homogeneous and bioturbated mud
Beds on confining topography (Paola Ridge)	Amantea Fan lobe	Paola ridge	PL	Parallel, low-amplitude reflections	52–51	Well stratified beds with laminated fine sands (F9)
Frontally-confined tabular beds	Amantea Fan lobe	Lower basin floor	PH	Parallel, high-amplitude reflections	50	Well stratified beds with massive medium sands with basal flame structures (F8f)
Bedforms (stoss side)	Amantea Fan lobe	Upper basin floor	CH	Large-scale convex, high-amplitude reflections	55	Well stratified beds with massive (F8m) to laminated fine sand (F9) with variable thickness
Scours	Amantea Fan lobe	Upper basin floor	SH	Structureless, highly reflective	56	Sporadically amalgamed beds with massive very coarse to coarse sands with basal flame structures (F5f) and laminated coarse sands (F7)

formation can be addressed: i) to the action of supercritical flows developing hydraulic jumps caused by flow expansion and thus representing the erosive portion characterizing the trough of cyclic steps, or ii) excavation of an initial bed defect involving flows, not necessarily supercritical, but thicker than the scour depth (Symons et al., 2016). According to our data, the first hypothesis is preferred here also considering the sedimentary facies identified in the turbidites filling the scour. The same facies have been recognized in channel–levee environments where scours, interpreted as related to the formation of large-scale cyclic steps, are filled by massive or normally graded infills, strong amalgamation, abundant rip-up clasts and soft-sediment deformations (Lang et al., 2017a; Ono and Plink-björklund, 2018; Cornard and Pickering, 2019). For these reasons, the scour is interpreted as the trough of erosional cyclic steps where the erosion, due to the occurrence of hydraulic jumps, is immediately followed by deposition of relatively amalgamed coarse-grained massive sands with mudclasts and basal flame structures (F5f in Fig. 9a). Since cyclic steps are characterized by upslope migration (Cartigny et al., 2014; Covault et al., 2017; Slootman and Cartigny, 2020), the occurrence of traction carpets below hydraulic jump deposits can thus eventually represent the deposits from the stoss side of an underlying cyclic step (Fig. 6, F7 in Fig. 9a).

Downflow, in the stoss side of a depositional bedform, part of a train with internal upslope migrating reflectors (Fig. 3d), consists of massive medium/fine-grained top-cut-out beds (turbidites 3, 4 and 5 in core 55, Fig. 7c). The depositional bedforms identified in the Amantea Fan lobe present morphometric characteristics that match the category of small-scale bedforms (Wynn and Stow, 2002; Symons et al., 2016). Generally, small-scale asymmetric upslope-migrating bedforms are associated with supercritical turbidity currents and in particular with cyclic step deposition (Cartigny et al., 2014; Postma and Cartigny, 2014; Symons et al., 2016; Lang et al., 2017a; Slootman and Cartigny, 2020). Similar architectures, where beck-sets are well visible and preserved (Fig. 5d), occur when the deposition on the stoss side exceeds erosion of the lee side reflecting high aggradation rates resulting in net-depositional cyclic steps (Kostic, 2011; Cartigny et al., 2014; Slootman and Cartigny, 2020). On the stoss side of cyclic steps, the flow is subcritical and prone to deposition (Fig. 6). Traction is the prevalent transport mechanism resulting in massive top-cut-out turbidites (Postma and Cartigny, 2014). Cyclic steps can present small-scale antidunes on their surface sometimes one order of magnitude smaller compared to cyclic steps (Zhong et al., 2015; Lang et al., 2017a, 2017b). A similar architecture could not be resolved by the resolution of sub-bottom seismic profiles. Moreover, the occurrence of massive sand can also be interpreted as deposits of stable antidunes with high aggradation rates (Lang et al., 2017a, 2017b). For this reason, it cannot be excluded the hypothesis that the described turbidites composing the bedform stoss side could belong to net-depositional antidunes. The facies in the bedforms of the Amantea Fan lobe conform therefore with a model of deposition associated with the stoss side of a net-depositional cyclic step or superimposed antidune on the surface of the cyclic step (Fig. 9a). In the lower basin floor of the Amantea fan, turbidity currents encounter the obstacle of the southern tip of the Paola Ridge. Numerical modeling (Nasr-Azadani et al., 2013; Nasr-Azadani and Meiburg, 2014; Howlett et al., 2019), tank experiments (Lane-Serff et al., 1995; Patacci et al., 2015; Soutter et al., 2021) and field studies (Kneller et al., 1991; Kneller and McCaffrey, 1999; Tinterri et al., 2016, 2022) on frontally-confined basins show that in approaching a counter-slope, turbidity currents decelerate, inflate and pass from supercritical to subcritical. Topographically-induced deceleration and possible hydraulic jumps (defined as upstream hydraulic jumps by Soutter et al., 2021) have been observed in tank experiments (Hamilton et al., 2017; Pohl et al., 2020; Soutter et al., 2021) and numerical modeling (Howlett et al., 2019). However, the relative deposits in sandy lobe or basin plain deposits have rarely been recognized in outcrops and in seismic studies (e.g., Tinterri et al., 2023). Massive facies and flame structures, characterizing the frontally-confined tabular beds at the base of the Paola ridge (turbidites 2, 3 and 5 in core 50, Fig. 8b), are indicative of the high fall-out rate of the basal dense part of the flow. Their facies could be a proof of hydraulic jumps associated with flow confinement and deceleration due to seafloor topography (Fig. 9b). Moreover, turbidites 2, 3 and 5 exhibit a normal grading trend, which records the passage and/or the partial collapse of the upper turbulent low-density part of the flow (Fig. 8b). In fact, when the current is completely blocked by a barrier, as in this case, the fluid velocities may be negative and thus resulting in a current "reflection" that propagates perpendicular to the reflecting surface (Kneller et al., 1991; Kneller, 1995; Kneller and Buckee, 2000; Patacci et al., 2015; Howlett et al., 2019). This interpretation is in agreement with the normally-graded fine-grained facies that can be related both to the deposition from a waning and depletive flow and a reflected and ponded turbidity current (Pickering and Hiscott, 1985; Felletti, 2002; Tinterri et al., 2016, 2022) (Fig. 9b).

Turbidity currents impacting above a morphologic high result in the progressive onlap of the beds against the barrier. Fieldwork studies revealed that the topographic confinement promotes the decoupling of the upper turbulent flow which can ascend the morphologic high and finally collapse depositing its fine-grained load on the slope of the high (Pickering and Hiscott, 1985; Kneller et al., 1991; Kneller and McCaffrey, 1999; Tinterri and Tagliaferri, 2015). Fine-grained turbidites with low regime tractive structures such as plane lamination (turbidite beds 1 to 5 in core 51, Fig. 8c) are found on the slope of the Paola ridge.

Fig. 8. (a) Correlation of cores 56–50–51–52 creating a transect in a NW–SE direction (locations in Fig. 1b). The correlation highlights that most of the beds onlap on the surface of the Paola Ridge and are absent in core 52. (b) Core 50 sampled tabular beds in the lower basin floor (Fig. 3c) where medium-grained turbidite beds occur, while (c) core 51 (located on the Paola Ridge) predominantly sampled thin-bedded fine-grained beds. Turbidite bed numbers are indicated in the yellow boxes to the left of the core photographs.

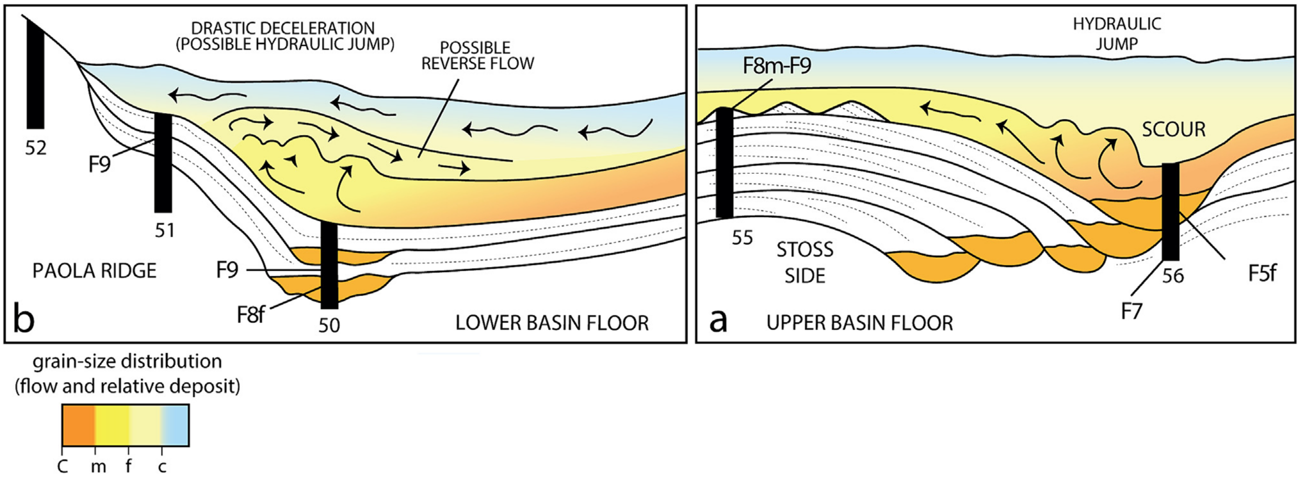

Fig. 9. Interpretation of the flow dynamics according to the sedimentological facies. (a) Cyclic step construction with supercritical flow on the lee side, resulting in traction carpets, hydraulic jump in the scour, equivalent to the massive facies, and subcritical flow on the stoss side where tractive structures occur. (b) Flow dynamic relative to the interaction between turbidity currents and frontal confinement possibly producing a hydraulic jump at the toe of the ridge (marked by massive facies with flame structures) and the production of a reverse flow.

Therefore, they substantiate that only the upper part of the flow reaches the slope of the high and forms low-density subcritical turbidity current (Postma and Cartigny, 2014; Tinterri et al., 2023).

In conclusion, Fig. 10 summarizes the effects of the various interactions between seafloor topography and turbidity flow dynamics and relative facies distribution. In the upper and steeper basin floor high-density erosive supercritical turbidity currents characterize the most proximal region of the fan lobe where erosive cyclic steps occur. Downslope, the still supercritical but aggrading turbidity currents result in prevalent depositional upslope-migrating cyclic steps with possible superimposition of antidunes. In the lower basin floor, less steep than the upper basin floor, the turbidity currents are interpreted to have a supercritical character, before returning into a subcritical stage passing through the hydraulic jump at the toe of the ridge. Finally, only low-density subcritical flows can overcome the frontal morphological obstacle represented by the Paola ridge and deposit on the associated counter-slope.

6. Conclusions

The lobe of the Amantea Fan is an example of a frontally confined sandy lobe, whose deposition occurred during the last falling stage, in which seafloor topography plays an important role in controlling the style of deposition. Interpretation of the lobe geometry and its internal stratifications allowed the identification of the feeder system coinciding with the Olivia Canyon. The interpretation of the seismic profiles and the analysis of the samples acquired on the surface of the lobe, parallel and perpendicular to the principal flow direction (SE–NW), resulted in the identification of different depositional styles. In the upper steep basin floor, the lobe is composed of erosional and depositional cyclic

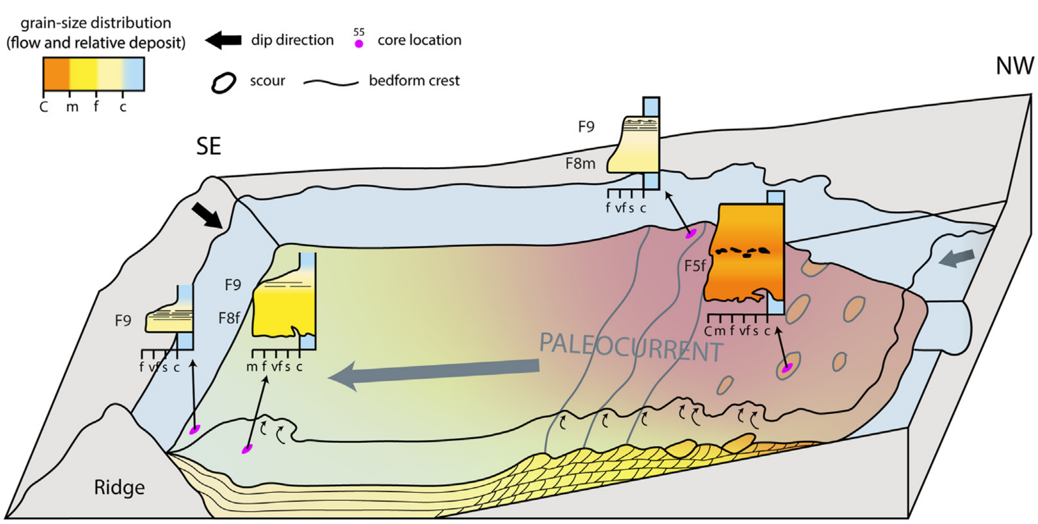

structural ridge	lower basin floor	upper basin floor	lower slope	SEAFLOOR MORPHOLOGY
subcritical flow / upstream hydraulic jump	supercritical flow	supercritical flow	flow expansion loose of competence	FLOW DYNAMICS
onlapping beds	tabular beds	depositional cyclic steps or antidunes / erosional cyclic steps	channel-mouth	GEOLOGICAL ELEMENTS

Fig. 10. Summary sketch of the different facies associations according to their different locations in the lobe. The graded colors represent the interpreted grain-size distribution inside the flows.

steps that evolve in the lower basin floor in tabular stratification that progressively onlap the surface of the Paola Ridge. For the first time, supercritical bedforms in a submarine lobe were identified in two distinct positions, in the scour of an erosional cyclic step and in the stoss side of a depositional cyclic step or antidune. Coarse to medium-grained massive sand with flame structures, generally associated with the occurrence of hydraulic jumps, has been identified in the scour of a cyclic step and at the toe of the ridge. The latter represents an example of a topographically induced hydraulic jump driven by frontal confinement, a phenomenon previously observed in tank experiments and numerical modeling and rarely in the field. Top-cut-out beds with massive basal facies and upper tractive structures compose the stoss side of a bedform interpreted as a net-depositional cyclic step or superimposed antidunes. The distance from the source area and the dip of the slope are here assumed as the major factors controlling the observed fan-lobe depositional style. Overall, the present study broadens the understanding of the range of processes that are driven by the interaction between turbidity currents and seafloor topography. The recognition that the topography influences the degree of criticality of the flow and consequently the morphodynamics and facies of the relative deposits may help to explain sediment distribution and improve depositional models of fan lobes in confined settings.

CRediT authorship contribution statement

E. Scacchia: Writing – original draft, Visualization, Methodology, Formal analysis, Data curation, Conceptualization. **R. Tinterri:** Writing – review & editing, Supervision, Resources. **F. Gamberi:** Writing – review & editing, Validation, Supervision, Investigation, Data curation.

Data availability

The authors do not have permission to share data.

Declaration of competing interest

The authors declare that they have no known competing financial interests or personal relationships that could have appeared to influence the work reported in this paper.

Acknowledgments

The authors wish to thank Sergio Longhitano, Gianluca Cornamusini, Salvatore Milli, Alessandro Amorosi, Marco Roveri, Vanni Pizzati and Simone Lombardi for precious and constructive discussions and advice. The authors also wish to thank Alessandra Mercorella, Andrea Gallerani, Fabio Savelli and Elisa Leidi for the processing and the management of the data. The authors also wish to thank the University of Parma for funding the PhD scholarship of ES, from whose thesis the paper has been extracted. The authors are also deeply grateful to the Editor Catherine Chaguè and the two anonymous reviewers for their very helpful comments and suggestions.

References

Amy, L.A., McCaffrey, W.D., Kneller, B.C., 2004. The influence of a lateral basin-slope on the depositional patterns of natural and experimental turbidity currents. Geological Society Special Publication 221, 311–330. https://doi.org/10.1144/GSL.SP.2004.221.01.17.

Bosman, A., Casalbore, D., Dominici, R., 2017. Cyclic steps at the head of channelized features along the Calabrian margin (Southern Tyrrhenian Sea, Italy). In: Guillén, J., Acosta, J., Chiocci, F., Palanques, A. (Eds.), Atlas of Bedforms in the Western Mediterranean. Springer, Cham, pp. 229–233 https://doi.org/10.1007/978-3-319-33940-5_35.

Cartigny, M.J.B., Postma, G., 2017. Turbidity current bedforms. In: Guillén, J., Acosta, J., Chiocci, F., Palanques, A. (Eds.), Atlas of Bedforms in the Western Mediterranean. Springer, Cham, pp. 29–33 https://doi.org/10.1007/978-3-319-33940-5_31.

Cartigny, M.J.B., Postma, G., van den Berg, J.H., Mastbergen, D.R., 2011. A comparative study of sediment waves and cyclic steps based on geometries, internal structures and numerical modeling. Marine Geology 280, 40–56. https://doi.org/10.1016/j.margeo.2010.11.006.

Cartigny, M.J.B., Ventra, D., Postma, G., van Den Berg, J.H., 2014. Morphodynamics and sedimentary structures of bedforms under supercritical-flow conditions: new insights from flume experiments. Sedimentology 61, 712–748. https://doi.org/10.1111/sed.12076.

Casalbore, D., Chiocci, F.L., Mugnozza, G.S., Tommasi, P., Sposato, A., 2011. Flash-flood hyperpycnal flows generating shallow-water landslides at Fiumara mouths in Western Messina Strait (Italy). Marine Geophysical Research 32, 257–271. https://doi.org/10.1007/s11001-011-9128-y.

Casalbore, D., Bosman, A., Domenico, R., Chiocci, F.L., 2014. Coastal and submarine landslides in the tectonically-active tyrrhenian Calabrian margin (Southern Italy): examp les and geohazard implications. Submarine Mass Movements and Their Consequences. Advances in Natural and Technological Hazards Research. 6th International Symposium vol. 37, pp. 201–212. https://doi.org/10.1007/978-3-319-00972-8.

Casalbore, D., Ridente, D., Bosman, A., Chiocci, F.L., 2017. Depositional and erosional bedforms in Late Pleistocene–Holocene pro-delta deposits of the Gulf of Patti (southern Tyrrhenian margin, Italy). Marine Geology 385, 216–227. https://doi.org/10.1016/j.margeo.2017.01.007.

Clementucci, R., Lafosse, M., Casalbore, D., Ridente, D., d'Acremont, E., Rabaute, A., Chiocci, F.L., Gorini, C., 2022. Common origin of coexisting sediment undulations and gullies? Insights from two modern Mediterranean prodeltas (southern Italy and northern Morocco). Geomorphology 402, 108–133. https://doi.org/10.1016/j.geomorph.2022.108133.

Cornard, P.H., Pickering, K.T., 2019. Supercritical-flow deposits and their distribution in a submarine channel system, Middle Eocene, Ainsa Basin, Spanish Pyrenees. Journal of Sedimentary Research 89, 576–597. https://doi.org/10.2110/jsr.2019.34.

Cornard, P.H., Pickering, K.T., 2020. Submarine topographic control on distribution of supercritical-flow deposits in lobe and related environments, middle eocene, Jaca basin, Spanish pyrenees. Journal of Sedimentary Research 90, 1222–1243. https://doi.org/10.2110/JSR.2020.59.

Corradino, M., Pepe, F., Bertotti, G., Picotti, V., Monaco, C., Nicolich, R., 2020. 3-D architecture and Plio-Quaternary evolution of the Paola Basin: insights into the forearc of the Tyrrhenian–Ionian subduction system. Tectonics 39, 1–24. https://doi.org/10.1029/2019TC005898.

Covault, J.A., Kostic, S., Paull, C.K., Sylvester, Z., Fildani, A., 2017. Cyclic steps and related supercritical bedforms: building blocks of deep-water depositional systems, western North America. Marine Geology 393, 4–20. https://doi.org/10.1016/j.margeo.2016.12.009.

Deptuck, M.E., Piper, D.J.W., Savoye, B., Gervais, A., 2008. Dimensions and architecture of late Pleistocene submarine lobes off the northern margin of East Corsica. Sedimentology 55, 869–898. https://doi.org/10.1111/j.1365-3091.2007.00926.x.

Fedele, J.J., Hoyal, D., Barnaal, Z., Tulenko, J., Awalt, S., 2016. Bedforms created by gravity flows. SEPM Special Publication 106, 95–121. https://doi.org/10.2110/sepmsp.106.12.

Felletti, F., 2002. Complex bedding geometries and facies associations of the turbiditic fill of a confined basin in a transpressive setting (Castagnola Fm., Tertiary Piedmont Basin, NW Italy). Sedimentology 49, 645–667. https://doi.org/10.1046/j.1365-3091.2002.00467.x.

Fildani, A., Normark, W.R., Kostic, S., Parker, G., 2006. Channel formation by flow stripping: large-scale scour features along the Monterey East Channel and their relation to sediment waves. Sedimentology 53, 1265–1287. https://doi.org/10.1111/j.1365-3091.2006.00812.x.

Fildani, A., Kostic, S., Covault, J.A., Maier, K.L., Caress, D.W., Paull, C.K., 2021. Exploring a new breadth of cyclic steps on distal submarine fans. Sedimentology 68, 1378–1399. https://doi.org/10.1111/sed.12803.

Gamberi, F., Marani, M., 2006. Hinterland geology and continental margin growth: the case of the Gioia Basin (southeastern Tyrrhenian Sea). Geological Society Special Publication 262, 349–363. https://doi.org/10.1144/GSL.SP.2006.262.01.21.

Gamberi, F., Marani, M., 2008. Controls on holocene deep-water sedimentation in the northern Gioia Basin, Tyrrhenian Sea. Sedimentology 55, 1889–1903. https://doi.org/10.1111/j.1365-3091.2008.00971.x.

Gamberi, F., Rovere, M., 2010. Mud diapirs, mud volcanoes and fluid flow in the rear of the Calabrian Arc Orogenic Wedge (southeastern Tyrrhenian Sea). Basin Research 22, 452–464. https://doi.org/10.1111/j.1365-2117.2010.00473.x.

Gamberi, F., Rovere, M., Mercorella, A., Leidi, E., 2014. The influence of a lateral slope on turbidite lobe development on a modern deep-sea slope fan (Villafranca deep-sea fan, Tyrrhenian Sea). Journal of Sedimentary Research 84, 475–486. https://doi.org/10.2110/jsr.2014.37.

Gamberi, F., Della Valle, G., Marani, M., Mercorella, A., Distefano, S., Di Stefano, A., 2019. Tectonic controls on sedimentary system along the continental slope of the central and southeastern Tyrrhenian Sea. Italian Journal of Geosciences 138, 317–332. https://doi.org/10.3301/IJG.2019.08.

Gong, C., Chen, L., West, L., 2017. Asymmetrical, inversely graded, upstream-migrating cyclic steps in marine settings: Late Miocene–early Pliocene Fish Creek–Vallecito Basin, southern California. Sedimentary Geology 360, 35–46. https://doi.org/10.1016/j.sedgeo.2017.09.002.

Hage, S., Cartigny, M.J.B., Clare, M.A., Sumner, E.J., Vendettuoli, D., Clarke, J.E.H., Hubbard, S.M., Talling, P.J., Gwyn Lintern, D., Stacey, C.D., Englert, R.G., Vardy, M.E., Hunt, J.E., Yokokawa, M., Parsons, D.R., Hizzett, J.L., Azpiroz-Zabala, M., Vellinga, A.J., 2018. How to recognize crescentic bedforms formed by supercritical turbidity currents in the geologic record: insights from active submarine channels. Geology 46, 563–566. https://doi.org/10.1130/G40095.1.

Hamilton, P., Gaillot, G., Strom, K., Fedele, J., Hoyal, D., 2017. Linking hydraulic properties in supercritical submarine distributary channels to depositional-lobe geometry. Journal of Sedimentary Research 87, 935–950. https://doi.org/10.2110/jsr.2017.53.

Hiscott, R.N., 1994. Traction-carpet stratification in turbidites - fact or fiction? Journal of Sedimentary Research A64, 204–208.

Howlett, D.M., Ge, Z., Nemec, W., Gawthorpe, R.L., Rotevatn, A., Jackson, C.A.L., 2019. Response of unconfined turbidity current to deep-water fold and thrust belt topography:

orthogonal incidence on solitary and segmented folds. Sedimentology 66, 2425–2454. https://doi.org/10.1111/sed.12602.
Huang, H., Imran, J., Pirmez, C., Zhang, Q., Chen, G., 2009. The critical densimetric froude number of subaqueous gravity currents can be non-unity or non-existent. Journal of Sedimentary Research 79, 479–485. https://doi.org/10.2110/jsr.2009.048.
Hughes Clarke, J.E., 2016. First wide-angle view of channelized turbidity currents links migrating cyclic steps to flow characteristics. Nature Communications 7, 1–13. https://doi.org/10.1038/ncomms11896.
Hughes Clarke, J.E., Shor, A., Piper, D.J.W., Mayer, L.A., 1990. Large-scale current-induced erosion and deposition in the path of the 1929 Grand Banks turbidity current. Sedimentology 37, 613–629. https://doi.org/10.1111/j.1365-3091.1990.tb00625.x.
Kneller, B., 1995. Beyond the turbidite paradigm: physical models for deposition of turbidites and their implications for reservoir prediction. Geological Society Special Publication 94, 31–49. https://doi.org/10.1144/GSL.SP.1995.094.01.04.
Kneller, B., Buckee, C., 2000. The structure and fluid mechanics of turbidity currents: a review of some recent studies and their geological implications. Sedimentology 47, 62–94. https://doi.org/10.1046/j.1365-3091.2000.047s1062.x.
Kneller, B., McCaffrey, W., 1999. Depositional effects of flow nonuniformity and stratification within turbidity currents approaching a bounding slope: deflection, reflection, and facies variation. Journal of Sedimentary Research 69, 980–991. https://doi.org/10.2110/jsr.69.980.
Kneller, B., Edwards, D., McCaffrey, W., Moore, R., 1991. Oblique reflection of turbidity currents. Geology 19, 250–252. https://doi.org/10.1130/0091-7613(1991)019<0250:OROTC>2.3.CO;2.
Komar, P.D., 1971. Hydraulic jumps in turbidity currents. Geological Society of Ameircan Bullettin 82, 1477–1488. https://doi.org/10.1130/0016-7606(1971)82.
Kostic, S., 2011. Modeling of submarine cyclic steps: controls on their formation, migration, and architecture. Geosphere 7, 294–304. https://doi.org/10.1130/GES00601.1.
Kostic, S., 2014. Upper flow regime bedforms on levees and continental slopes: turbidity current flow dynamics in response to fine-grained sediment waves. Geosphere 10, 1094–1103. https://doi.org/10.1130/GES01015.1.
Kostic, S., Casalbore, D., Chiocci, F., Lang, J., Winsemann, J., 2019. Role of upper-flow-regime bedforms emplaced by sediment gravity flows in the evolution of deltas. Journal of Marine Science and Engineering 9, 1–29. https://doi.org/10.3390/jmse7010005.
Lane-Serff, G.F., Beal, L.M., Hadfield, T.D., 1995. Gravity current flow over obstacles. Fluid Mechanics 292, 39–53. https://doi.org/10.1017/S002211209500142X.
Lang, J., Winsemann, J., 2013. Lateral and vertical facies relationships of bedforms deposited by aggrading supercritical flows: from cyclic steps to humpback dunes. Sedimentary Geology 296, 36–54. https://doi.org/10.1016/j.sedgeo.2013.08.005.
Lang, J., Brandes, C., Winsemann, J., 2017a. Erosion and deposition by supercritical density flows during channel avulsion and backfilling: field examples from coarse-grained deep-water channel–levée complexes (Sandino Forearc Basin, southern Central America). Sedimentary Geology 349, 79–102. https://doi.org/10.1016/j.sedgeo.2017.01.002.
Lang, J., Sievers, J., Loewer, M., Igel, J., Winsemann, J., 2017b. 3D architecture of cyclic-step and antidune deposits in glacigenic subaqueous fan and delta settings: integrating outcrop and ground-penetrating radar data. Sedimentary Geology 362, 83–100. https://doi.org/10.1016/j.sedgeo.2017.10.011.
Lo Iacono, C., Cartigny, M.J.B., Rizzo, E., Agate, M., Sulli, A., 2017. Potential cyclic steps in a gully system of the Gulf of Palermo (Southern Tyrrhenian Sea). In: Guillén, J., Acosta, J., Chiocci, F., Palanques, A. (Eds.), Atlas of Bedforms in the Western Mediterranean. Springer, Cham, pp. 235–240 https://doi.org/10.1007/978-3-319-33940-5.
Lowe, D.R., 1982. Sediment gravity flows: II. Depositional models with special reference to the deposits of high-density turbidity currents. Journal of Sedimentary Research 52, 279–297.
Milia, A., Turco, E., Pierantoni, P.P., Schettino, A., 2009. Four-dimensional tectono-stratigraphic evolution of the Southeastern peri-Tyrrhenian basins (Margin of Calabria, Italy). Tectonophysics 476, 41–56. https://doi.org/10.1016/j.tecto.2009.02.030.
Mutti, E., 1992. Turbidite Sandstones. Agip-Istituto di Geologia, Università di Parma, San Donato Milanese.
Mutti, E., Normark, W.R., 1987. Comparing examples of modern and ancient turbidite systems: problems and concepts. Marine Clastic Sedimentology 1–38.
Mutti, E., Tinterri, R., Benevelli, G., Di Biase, D., Cavanna, G., 2003. Deltaic, mixed and turbidite sedimentation of ancient foreland basins. Marine and Petroleum Geology 20, 733–755. https://doi.org/10.1016/j.marpetgeo.2003.09.001.
Nasr-Azadani, M.M., Meiburg, E., 2014. Influence of seafloor topography on the depositional behavior of bi-disperse turbidity currents: a three-dimensional, depth-resolved numerical investigation. Environmental Fluid Mechanics 14, 319–342. https://doi.org/10.1007/s10652-013-9292-5.
Nasr-Azadani, M.M., Hall, B., Meiburg, E., 2013. Polydisperse turbidity currents propagating over complex topography: comparison of experimental and depth-resolved simulation results. Computers and Geosciences 53, 141–153. https://doi.org/10.1016/j.cageo.2011.08.030.
Normark, W.R., 1970. Growth patterns of deep-sea fans. American Association of Petroleum Geologists Bulletin 54, 2170–2195. https://doi.org/10.1306/5d25cc79-16c1-11d7-8645000102c1865d.
Normark, W.R., 1978. Fan valleys, channels, and depositional lobes on modern submarine fans: characters for recognition of sandy turbidite environments. AAPG Bulletin 62, 912–931. https://doi.org/10.1306/c1ea4f72-16c9-11d7-8645000102c1865d.
Ono, K., Plink-björklund, P., 2018. Froude supercritical flow bedforms in deepwater slope channels? Field examples in conglomerates, sandstones and fine-grained deposits. Sedimentology 65, 639–669. https://doi.org/10.1111/sed.12396.
Ono, K., Plink-Björklund, P., Eggenhuisen, J.T., Cartigny, M.J.B., 2021. Froude supercritical flow processes and sedimentary structures: new insights from experiments with a wide range of grain sizes. Sedimentology 68, 1328–1357. https://doi.org/10.1111/sed.12682.
Patacci, M., Haughton, P.D.W., McCaffrey, W.D., 2015. Flow behavior of ponded turbidity currents. Journal of Sedimentary Research 85, 903–936. https://doi.org/10.2110/jsr.2015.59.
Pickering, K.T., Hiscott, R.N., 1985. Contained (reflected) turbidity currents from the Middle Ordovician Cloridorme Formation, Quebec, Canada: an alternative to the antidune hypothesis. Deep-Water Turbidite Systems 32, 373–394. https://doi.org/10.1002/9781444304473.ch7.
Pohl, F., Eggenhuisen, J.T., Cartigny, M.J.B., Tilston, M.C., de Leeuw, J., Hermidas, N., 2020. The influence of a slope break on turbidite deposits: an experimental investigation. Marine Geology 424, 106–160. https://doi.org/10.1016/j.margeo.2020.106160.
Postma, G., Cartigny, M.J.B., 2014. Supercritical and subcritical turbidity currents and their deposits — a synthesis. Geology 42, 987–990. https://doi.org/10.1130/G35957.1.
Postma, G., Kleverlaan, K., 2018. Supercritical flows and their control on the architecture and facies of small-radius sand-rich fan lobes. Sedimentary Geology 364, 53–70. https://doi.org/10.1016/j.sedgeo.2017.11.015.
Postma, G., Cartigny, M., Kleverlaan, K., 2009. Structureless, coarse-tail graded Bouma Ta formed by internal hydraulic jump of the turbidity current? Sedimentary Geology 219, 1–6. https://doi.org/10.1016/j.sedgeo.2009.05.018.
Postma, G., Kleverlaan, K., Cartigny, M.J.B., 2014. Recognition of cyclic steps in sandy and gravelly turbidite sequences, and consequences for the Bouma facies model. Sedimentology 61, 2268–2290. https://doi.org/10.1111/sed.12135.
Postma, G., Hoyal, D.C., Abreu, V., Cartigny, M., Demko, T., Fedele, J., Kleverlaan, K., Pederson, K.H., 2016. Morphodynamics of supercritical turbidity currents in the channel–lobe transition zone. Submarine Mass Movements and Their Consequences. Advances in Natural and Technological Hazards Research vol. 41, pp. 469–478. https://doi.org/10.1007/978-3-319-20979-1.
Postma, G., Lang, J., Hoyal, D.C., Fedele, J.J., Demko, T., Abreu, V., Pederson, K.H., 2021. Reconstruction of bedform dynamics controlled by supercritical flow in the channel–lobe transition zone of a deep-water delta (Sant Llorenç del Munt, north-east Spain, Eocene). Sedimentology 68, 1674–1697. https://doi.org/10.1111/sed.12735.
Remacha, E., Fernández, L.P., Maestro, E., 2005. The transition between sheet-like lobe and basin-plain turbidites in the Hecho (south-central Pyrenees, Spain). Journal of Sedimentary Research 75, 798–819. https://doi.org/10.2110/jsr.2005.064.
Rovere, M., Gamberi, F., Mercorella, A., Rashed, H., Gallerani, A., Leidi, E., Marani, M., Funari, V., Pini, G.A., 2014. Venting and seepage systems associated with mud volcanoes and mud diapirs in the southern Tyrrhenian Sea. Marine Geology 347, 153–171. https://doi.org/10.1016/j.margeo.2013.11.013.
Sabato, L., Tropeano, M., 2004. Fiumara: a kind of high hazard river. Physics and Chemistry of the Earth 29, 707–715. https://doi.org/10.1016/j.pce.2004.03.008.
Scacchia, E., 2023. Turbidites Dominated by Supercritical Flows and Hydraulic Jumps in Relation to Morphologic Variations in Tectonically Controlled Basins. University of Parma, pp. 1–175 (Ph.D. thesis).
Scacchia, E., Tinterri, R., Gamberi, F., 2022. The influence of channel planform and slope topography on turbidity current overbank processes: the example of the Acquarone Fan (Southern Tyrrhenian Sea). Frontiers in Earth Science - Sedimentology, Stratigraphy and Diagenesis 9, 1–22. https://doi.org/10.3389/feart.2021.785164.
Sequeiros, O.E., 2012. Estimating turbidity current conditions from channel morphology: a Froude number approach. Journal of Geophysical Research: Oceans 117, 1–19. https://doi.org/10.1029/2011JC007201.
Shanmugam, G., Moiola, R.J., 1988. Submarine fans: characteristics, models, classification, and reservoir potential. Earth Science Reviews 24, 383–428. https://doi.org/10.1016/0012-8252(88)90064-5.
Slootman, A., Cartigny, M.J.B., 2020. Cyclic steps: review and aggradation-based classification. Earth-Science Reviews 201, 1–30. https://doi.org/10.1016/j.earscirev.2019.102949.
Sohn, Y.K., 1997. On traction-carpet sedimentation. Journal of Sedimentary Research 67, 502–509. https://doi.org/10.1306/d42685ae-2b26-11d7-8648000102c1865d.
Soutter, E.L., Bell, D., Cumberpatch, Z.A., Ferguson, R.A., Spychala, Y.T., Kane, I.A., Eggenhuisen, J.T., 2021. The influence of confining topography orientation on experimental turbidity currents and geological implications. Frontiers in Earth Science 8. https://doi.org/10.3389/feart.2020.540633.
Spinewine, B., Sequeiros, O.E., Garcia, M.H., Beaubouef, R.T., Sun, T., Savoye, B., Parker, G., 2009. Experiments on wedge-shaped deep sea sedimentary deposits in minibasins and/or on channel levees emplaced by turbidity currents. Part II. Morphodynamic evolution ofthe wedge and of the associated bedforms. Journal of Sedimentary Research 79, 608–628. https://doi.org/10.2110/jsr.2009.065.
Symons, W.O., Sumner, E.J., Talling, P.J., Cartigny, M.J.B., Clare, M.A., 2016. Large-scale sediment waves and scours on the modern seafloor and their implications for the prevalence of supercritical flows. Marine Geology 371, 130–148. https://doi.org/10.1016/j.margeo.2015.11.009.
Tinterri, R., Civa, A., 2021. Laterally accreted deposits in low efficiency turbidites associated with a structurally-induced topography (Oligocene Molare Group, Tertiary Piedmont Basin, NW Italy). Journal of Sedimentary Research 91, 751–772. https://doi.org/10.2110/jsr.2020.174.
Tinterri, R., Tagliaferri, A., 2015. The syntectonic evolution of foredeep turbidites related to basin segmentation: facies response to the increase in tectonic confinement (Marnoso-arenacea Formation, Miocene, Northern Apennines, Italy). Marine and Petroleum Geology 67, 81–110. https://doi.org/10.1016/j.marpetgeo.2015.04.006.
Tinterri, R., Muzzi Magalhaes, P., Tagliaferri, A., Cunha, R.S., 2016. Convolute laminations and load structures in turbidites as indicators of flow reflections and decelerations against bounding slopes. Examples from the Marnoso-arenacea Formation (northern Italy) and Annot Sandstones (south eastern France). Sedimentary Geology 344, 382–407. https://doi.org/10.1016/j.sedgeo.2016.01.023.
Tinterri, R., Laporta, M., Ogata, K., 2017. Asymmetrical cross-current turbidite facies tract in a structurally-confined mini-basin (Priabonian–Rupelian, Ranzano Sandstone, northern Apennines, Italy). Sedimentary Geology 352, 63–87. https://doi.org/10.1016/j.sedgeo.2016.12.005.

Tinterri, R., Mazza, T., Magalhaes, P.M., 2022. Contained-reflected megaturbidites of the Marnoso-arenacea Formation (Contessa Key Bed) and Helminthoid Flysches (Northern Apennines, Italy) and Hecho Group (South-Western Pyrenees). Frontiers in Earth Science 10, 1–31. https://doi.org/10.3389/feart.2022.817012.

Tinterri, R., Pizzati, V., Scacchia, E., 2023. Turbidite facies tracts as related to flow criticality and efficiency in tectonically confined basins: an outcrop perspective. 1st In-person Bouma Deep Water Geoscience Conference - Utrecht, Netherlands, Abstract Book, p. 8.

Trincardi, F., Correggiari, A., Field, M.E., Nomark, W.R., 1995. Turbidite deposition from multiple sources: Quaternary Paola Basin (eastern Tyrrhenian Sea). Journal of Sedimentary Research B: Stratigraphy Global Studies 65, 469–483. https://doi.org/10.1306/d4268289-2b26-11d7-8648000102c1865d.

Walker, R., 1965. The origin and significance of the internal sedimentary structures of turbidites. Proceedings of the Yorkshire Geological Society 35, 1–32.

Wentworth, C.K., 1922. A scale of grade and class terms for clastic sediments. The Journal of Geology 30, 377–392.

Wynn, R.B., Stow, D.A.V., 2002. Classification and characterisation of deep-water sediment waves. Marine Geology 192, 7–22. https://doi.org/10.1016/S0025-3227(02)00547-9.

Zhong, G., Cartigny, M.J.B., Kuang, Z., Wang, L., 2015. Cyclic steps along the South Taiwan Shoal and West Penghu submarine canyons on the northeastern continental slope of the South China Sea. Bulletin of the Geological Society of America 127, 804–824. https://doi.org/10.1130/B31003.1.